J. Astrophys. Astr. (1997) **18**, 415–433

Redshift Quantization in the Cosmic Background Rest Frame

W. G. Tifft[1], *National Radio Astronomy Observatory[2] Green Bank, West Virginia 24944, USA; Steward Observatory, University of Arizona, Tucson, Arizona 85721, USA*

Abstract. Evidence for redshift quantization is reviewed and summarized. The cosmic background rest frame appears to be central to the effect. Periods are consistently found to be members of a set predicted by the ninth-root Lehto-Tifft rule which has implications relating to the possible nature of time, particle physics and cosmology. Galaxies can be divided into four morphological families associated with particular classes of periods. Numerous examples are given including recent work where redshifts appear to show evidence of changes between related quantized levels.

Key words. Red shift—galaxies—cosmology.

1. Introduction

My redshift work began in 1970 with initial glimpses of unexpected properties of the redshift. Correlations were found which implied that the redshift could be an *intrinsic* property of galaxies. Further work uncovered suggestions of a granular 'quantized' structure in the redshift. The concept of galaxies as quantized structures connected to a fundamental redshift interval near $72\,\mathrm{km\,s^{-1}}$ was published in three papers (Tifft 1976, 1977a, b) in the mid 1970s. In the 1980s precise 21 cm radio data suggested that a comprehensive global quantization pattern existed. By the late 1980s there was evidence that the redshift was not only quantized, but possibly variable as well (Tifft 1988); several underlying periods were apparent (Tifft 1991). The initial phase, to 1992, is summarized in a 1995 review (Tifft 1995); Fig. 1 is a graphical view of the development with key references.

In 1992, at the suggestion of John Cocke, we examined the connection between the cosmic background radiation (CBR) rest frame and global quantization. We found a much richer pattern than seen in galactocentric studies. In 1993 a more dramatic change occurred. In a subject as controversial as redshift quantization, the normal reaction is that it must be wrong. Bill Napier, working with Bruce Guthrie in England found quite the opposite (Guthrie 1991, 1996), they confirmed effects among spiral galaxies viewed in the galactocentric rest frame. The controversy (Beardsley 1992) came to the attention of Ari Lehto in Finland who had developed a model which could predict precise redshift periods Lehto (1990). The marriage of the CBR rest

[1] This work was carried out while on sabbatical leave from Steward Observatory, University of Arizona.

[2] The National Radio Astronomy Observatory is a facility of the National Science Foundation, operated under cooperative agreement by Associated Universities, Inc.

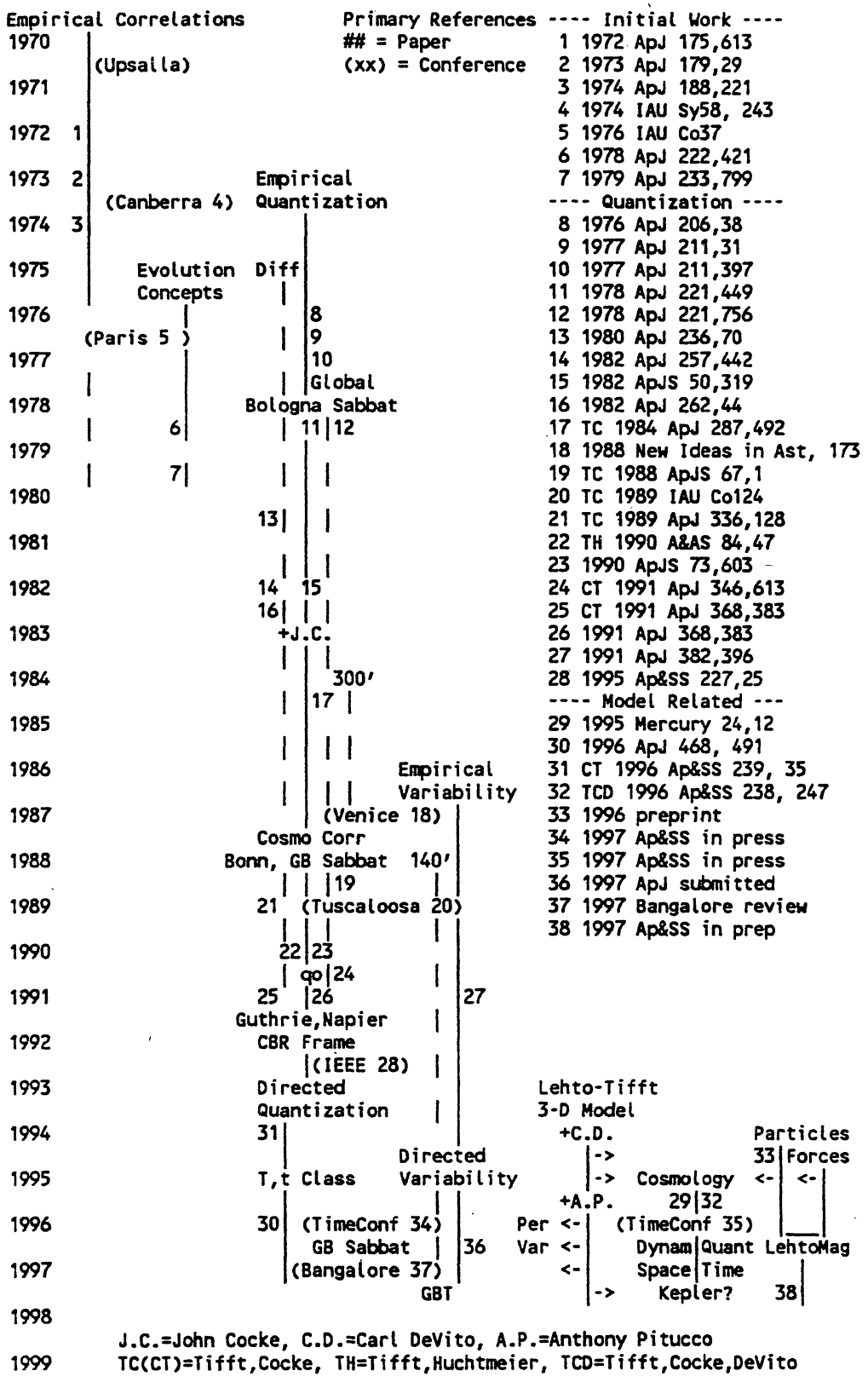

Figure 1. A graphical history of the development of redshift quantization ideas with the principal references.

frame with predicted periods developed from Lehto's work has completely reconfigured the study of redshift quantization.

The first aspect of recent work involves verification of the CBR rest frame and periodicity predictions. Other aspects apply the underlying theme, in Lehto's work, that *time* has a quantized three-dimensional structure. From this general concept we can develop a new cosmological model on the macroscopic scale, and a model of the underlying nature of the fundamental particles and forces on the microscopic scale. We do not have time here to discuss most of the published material from the early phase of quantization work. Key elements of the newer verification work are also available in the literature (Cocke & Tifft 1996; Tifft 1996, 1997); reviews of the evidence for quantization and the associated cosmology will appear in the proceedings of the conference on Time in Physics and Cosmology held in Tucson in April 1996 (Tifft 1996a, b). Important aspects related to fundamental particles and forces have not yet been discussed in the literature but can only be mentioned briefly in this short review. Patterns exist which suggest an underlying 'dynamical' substructure within 3-d time which may relate the forces, classes of particles, and their mass energies.

2. Data, procedures, and rest frames

Redshift quantization was discovered using optical redshifts but only 21 cm redshifts achieve the precision required to actively pursue the subject. A single-dish 21 cm observation yields a heliocentric redshift, V_h, a profile width, W, a flux, F, an asymmetry or shape parameter, A, and a signal-to-noise measure, S/N. Asymmetry indices are available only in work by Tifft and Cocke, and only a few data sets provide signal-to-noise values. The flux-to-width ratio, F/W, is substituted in some cases. When multiple epoch data are available the (new–old) redshift provides a 'Deviation' measure used in uncertainty and variability studies. Definitions of parameters are given in several references (Tifft & Cocke 1988; Tifft 1990).

Extensive studies of the precision of 21 cm data exist. Detailed studies by Tifft and Huchtmeier (1990) and Tifft (1990), finds consistent sub-km s^{-1} repeatability for redshifts above S/N of 10. Random error varies as the square-root of the bandwidth used and is *not* dependent on profile width given adequate S/N. Standards have been established and different radio telescopes compared. Barring small operating system errors, easily eliminated, *no* systematic errors are found in 21 cm data. There are small resolution effects (Tifft 1991). Only a few large surveys are suitable for quantization work. These include Fisher-Tully (1981); Tifft-Cocke (1988); and Tifft (1990) surveys, some older work with the NRAO 300 foot telescope and major Arecibo surveys (Hoffmann *et al.* 1987; Giovanelli & Haynes 1985; Bicay & Giovanelli 1986).

The quantization model implies that galaxies have an internal quantized substructure; they must be carefully sampled. Just as one should not mix atomic species in spectral analysis, one must distinguish galaxy types in quantization work. The early global studies distinguished between dwarf galaxies and luminous spirals (Tifft 1978; Tifft & Cocke 1984). Even within the spirals some distinction is important. The earliest work used 21 cm profile width to discriminate. From the Fisher-Tully relationship we know this is appropriate. Now widths are combined with

morphology, using deVaucouleur's t index. This is especially important to separate dwarfs which have distinct quantization properties. Given a homogeneous set, data quality is controlled with S/N or F/W. In recent work on variability the asymmetry index may distinguish stages of change. Subdividing introduces degrees of freedom and degrades significance, but is essential. *Quantization is an intrinsic type-dependent property of galaxies.*

Redshift quantization generates a global periodic pattern in an appropriate rest frame. Periods appear as 'phase' concentrations when redshifts from homogeneous samples are divided by appropriate periods,

$$V_{\mathrm{corr}}/P = n.\phi.$$

ϕ is phase, P the period, and V_{corr} the observed redshift referred to a rest frame and corrected for cosmological non-linearity. Spectral power analysis is used to detect and evaluate periodicities. Power in a standard power spectrum is exponentially distributed about a mean of unity. For an ideal distribution the probability of finding a given power, w, at a specified period is e^{-w}. We find consistent high power associated with specific periods predicted by our model. Since extreme value statistics with modest sized samples has been questioned, recent work has used Monte Carlo simulations to verify significance. Binomial statistics has also been used to show unique concentrations of power at predicted periods. The methods have been extensively discussed (Guthrie & Napier 1996; Tifft 1996; Lake & Roeder 1972).

Redshift quantization appears consistently only when redshifts are transformed to a specific rest frame. Virtually all instrumental or processing errors are ruled out by this association. The original rest frame was galactocentric, $(232.4, -36.6, 0.9)\,\mathrm{km\,s^{-1}}$ in galactic coordinates, and has not varied much since derived in the 1980s (Tifft & Cocke 1984). The numbers are the tangential, radial (+inward), and vertical (+ = North) motions of the Sun within the Galaxy. Only certain classes of galaxies, notably local spirals, show clear quantization in this frame. More general and consistent periodicities appear in the cosmic background radiation rest frame. Our adopted transformation is $(-243, -31, 275)\,\mathrm{km\,s^{-1}}$ (Tifft 1996), close to the COBE dipole vertex of the CBR.

Transformations are evaluated by mapping power, at a given period, over a range of the components and examining power contours. Fig. 2 shows an example for a Virgo cluster sample where power is maximized near the COBE CBR dipole vertex (box in upper frame), but shows no association with the galactic center ($\times$ in lower frame). Power, scaled by 10, is shown as a function of the tangential, θ, and radial, π, transformation components at a fixed perpendicular, Z, value. Many samples consistently associate with the CBR. Searches over wide ranges show that power peaks like those near the CBR vertex rarely occur by accident; the consistent appearance of peaks at the vertex indicates the significance and cosmological association of redshift quantization. Using this association and predicted periods we can now subdivide galaxies into specific quantization families.

Multiple rest frames are not consistent with ordinary dynamics. In quantization models the CBR dipole is not due to random motion of our galaxy since random motion between galaxies will destroy quantization by projection effects. This was already known from galaxy pairs where quantization is inconsistent with orbital motion (Tifft & Cocke 1989). Quantization rules out significant *spatial* motion between galaxies. The main galactocentric period is at or close to the $36.6\,\mathrm{km\,s^{-1}}$ period predicted by current models. The period was first seen by Tifft and Cocke

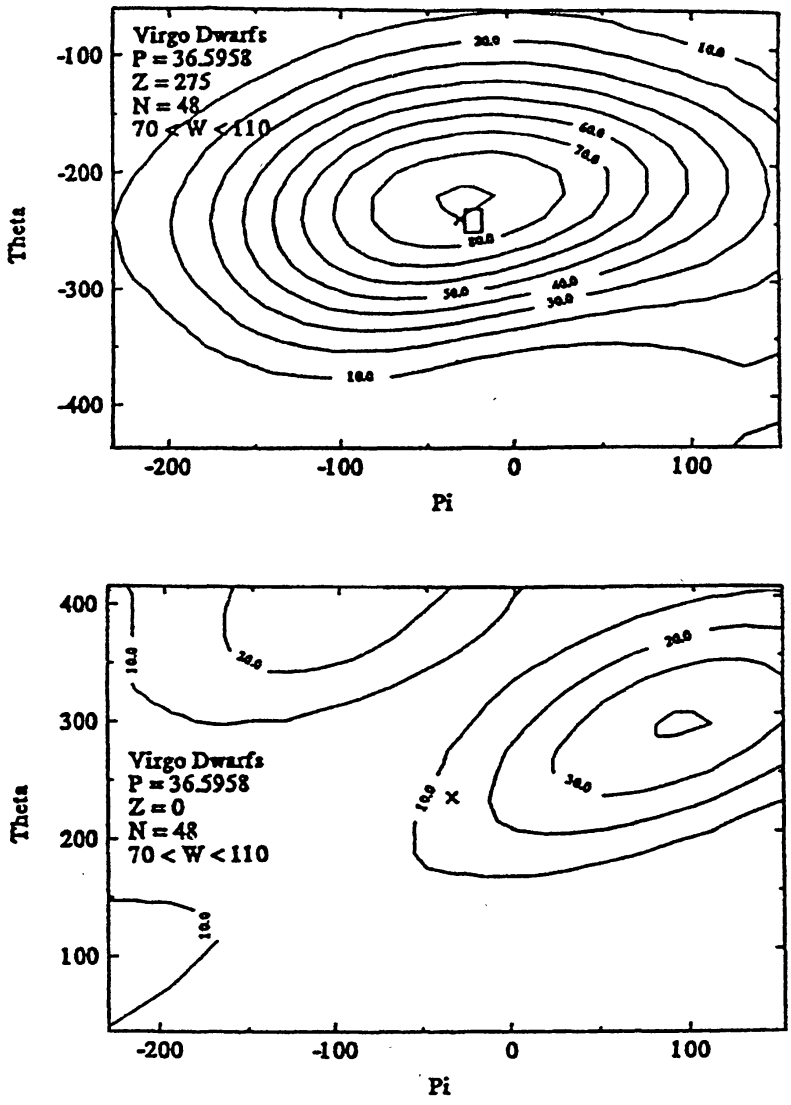

Figure 2. Power contours for transformations to the cosmocentric (upper) or galactocentric (lower) frames for a Virgo cluster sample.

(1984) among galaxies with wide 21 cm profiles. Guthrie and Napier (1991, 1996) (GN) subsequently found a similar period for local spirals of all types if non-spiral dwarfs are excluded. Figure 3 (top) shows periodicity in the original GN sample in a phase-profile width diagram using our galactocentric transformation and predicted period; a double cycle is used to show the phase clumping. The lower frame contains higher redshift Sc galaxies within the local supercluster. Again one can see periodic clumping. The periodicity is present for homogeneous samples but does not phase together overall.

Recent work by Guthrie and Napier (1996) detects strong periodicities at a variety of associated vertices near the galactic center. Figure 4 is an analysis of one of their samples; the locations of major power maxima for an 18.8 km s^{-1} period (one half of the GN period) are shown with filled symbols sized according to peak power. Open triangles and squares show related peaks discussed by Guthrie and Napier. An X marks our galactic center vertex; the cross and open circle mark points, in the galactic

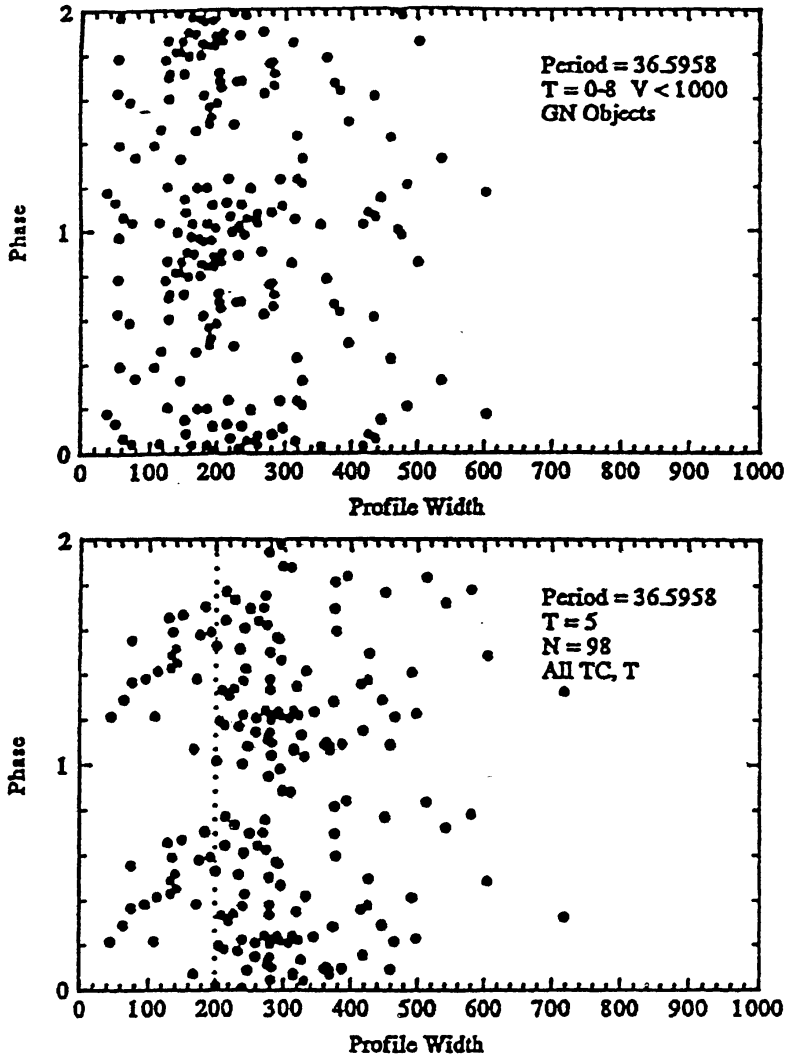

Figure 3. Phase-width plots for galaxy samples in the galactocentric frame. Homogeneous sets show the 36.6 km/s period with phase shifts.

plane, *opposite* the CBR dipole vertex from our work and COBE. Power concentrates near the CBR related location, not the galactic one. We believe the strong effects seen by Guthrie-Napier are *fluctuations* induced by a more basic cosmocentric effect. The dominate cosmocentric period for ordinary spirals is 18.3 km s^{-1}. The transverse components in the two transformations are nearly equal and opposite; the radial terms are nearly equal. We suspect there is a relationship between the two transformations and the rotational dynamics of the Galaxy. The cosmocentric form may incorporate the galactocentric form within it. The most effective transformations involve a relativistic transformation to the galactic center but a Galilean transformation to the CBR. Relativistic spatial velocity is certainly involved within the Galaxy; the cosmocentric link is different.

The galactocentric connection can be seen in some specific samples, or through the intense fluctuations found by Guthrie and Napier. The cosmocentric connection is much more consistent from sample to sample. Fig. 5 contains *eight* independent examples. Power contours (scaled by 10) are shown for periods and samples as

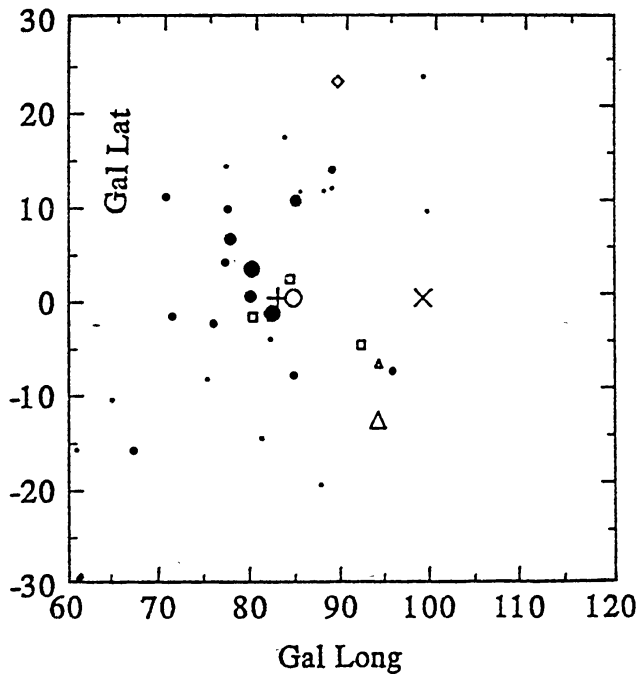

Figure 4. Power fluctuations, for a sample of local galaxies at an 18.8 km/s period, when redshifts are transformed to the vicinity of the galactic center. Fluctuations concentrate around the point opposite the cosmocentric longitude (+, ○) rather than the galactocentric location (×).

indicated. Axes are the transverse and radial transformation components, in km s^{-1}, at constant Z, usually 275 km s^{-1}. An X marks our standard vertex; the box, or portion thereof, is the COBE CBR dipole vertex error box.

At upper left local dwarfs with 21 cm profiles < 75 km s^{-1} wide represent extreme dwarf galaxies where periods related to 10.67 km s^{-1} dominate (Tifft 1996a). At upper right we see 249 common spirals with data in common between Fisher-Tully and Tifft-Cocke measurements. These are ordinary spirals, like ones used by Guthrie and Napier, with profile widths between 100 and 300 km s^{-1}. For such galaxies 18.3 and 36.6 km s^{-1} periods are dominate. The left central frames repeat the Virgo cluster sample from Fig. 2, and show local supercluster galaxies in the foreground of the Cancer supercluster. These Arecibo measures cover objects much like the local common spirals and show the same 36.6 km s^{-1} or related periods. This basic family appears again at $P = 18.3$ km s^{-1} in the two lower frames where Perseus supercluster data from Arecibo surveys are used. *Similar galaxies in separate samples are consistent!*. The Perseus examples show another effect. At lower right we have 179 galaxies with profile widths < 400 km s^{-1}. At lower left 53 galaxies with $W > 400$ km s^{-1} show a continuity of period and vertex. Such continuity is not likely by accident. Roughly 750 independent galaxies contribute to Fig. 5; we are not dealing with small numbers.

Resolution and contour shape depends on the distribution of galaxies on the sky and the period involved. Clustered Virgo galaxies have little global resolution. For short periods, in deep or widespread samples, the resolution is much higher. The two frames at right center show wide profile objects where short periods related to 5.76 km s^{-1} dominate. Local galaxies at the top, and Cancer supercluster galaxies

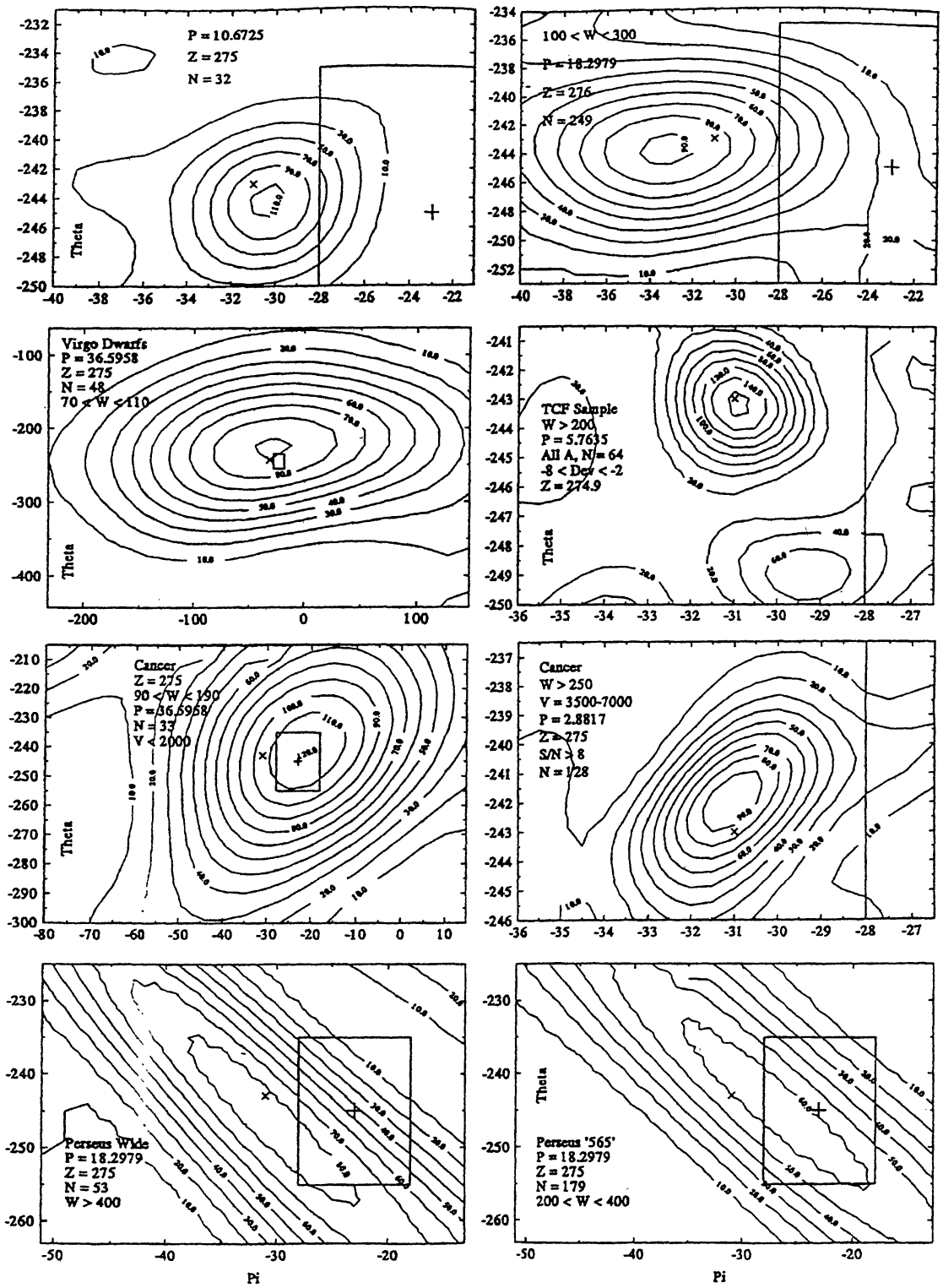

Figure 5. Power contours for eight galaxy samples when redshifts are transformed to the vicinity of the cosmic background dipole vertex (box). Samples within characteristic profile width ranges, but from different locations, are optimally periodic at predicted periods in the cosmocentric frame.

below, sharply define the vertex. The local sample peaks at power 17. Short periods in deep surveys provide an important check on cosmological corrections applied to redshifts. We find consistent matches at predicted periods for many samples, from independent regions and surveys, when referred to a consistent vertex associated with the CBR dipole. It seems incredibly unlikely that redshift quantization can be an accident. Most of the samples used here are discussed in the literature (Tifft 1996; 1996a).

3. The period model and galaxy families

Initial empirical work involved a $72\,\mathrm{km\,s^{-1}}$ period and simple relatives, notably $36\,\mathrm{km\,s^{-1}}$. Variability work introduced shorter periods, including 10.67 and $5.33\,\mathrm{km\,s^{-1}}$, and suggested that more complex underlying periods existed. While this work was proceeding, Ari Lehto was developing a model involving quantized time and energy which could represent mass energies, and other properties, of fundamental particles, the electron in particular. He noted that quantized time intervals in his work could match intervals (periods) in the redshift work. Initial tests for the predicted periods in redshift samples viewed in the CBR rest frame revealed an extraordinary agreement. Subsequent investigations have led to the development of a set of equations which represents both redshifts and particle mass-energies,

$$P_L = c2^{-(N/3)} = c2^{-(3D+L/3)} \quad E_{\mathrm{ferm}} = E_o 2^{-(N/3)} = E_o 2^{-(3D+M/3)},$$
$$P_T = c2^{-(N/9)} = c2^{-(9D+T/9)} \quad E_{\mathrm{boso}} = E_o 2^{-(N/4)} = E_o 2^{-(4D+F/4)}.$$

Two additional equations, scaled versions of the energy equations on the right, are required to describe the common particle mass-energies.

To derive the equations (Lehto 1990; Tifft 1996) one begins with the Planck time as a quantized unit to define units of length, energy, mass, and 'velocity',

$$t_o = 1/\nu_o, \quad l_o = ct_o, \quad E_o = h\nu_o, \quad m_o = E_o/c^2, \quad V_o = l_o/t_o = c.$$

One then allows these units to evolve by a doubling process, integral powers of two, common to many well known physical processes. If the process was that simple then ratios of various fundamental masses, energies, times, etc. should be powers of two. This is not the case, but Lehto noted that they did seem to associate with powers of $N/3$. He made the rather remarkable assumption that the doubling process might occur in a three dimensional volumetric sense, and be reduced to our level of one-dimensional perception by a cuberoot scalar operation. From this beginning a picture of time as having an underlying three dimensional geometry has begun to emerge at both the macroscopic (cosmological) and microscopic (particles and forces) level. Quantum physics associates with a three-dimensional quantized temporal geometry, and ordinary dynamics with continuous space.

The integer powers of two are written as a doubling part, D and a fractional part, L, T, M, or F to distinguish 'families' of roots. The first equation has three 'cube-root' families which forms independent doubling sequence. Two modifications to the cube root rule complete an introduction to the Lehto-Tifft equations. The first, relevant to particle physics, relates to forces, and associated bosons, using a fourth root reduction since force involves energy (3-d) acting over a fourth (spatial)

dimension. The remarkable success of this approach in representing bosonic masses and the forces is beyond the scope of this redshift review.

The second modification involves redshifts. To represent all periods the cube root rule becomes a ninth-root rule. Volume doubling assumes that all axes scale together by the cube root of two. Individual or asynchronous scaling generates ninth roots. Pure power-of-two, $T = 0$, periods (in velocity units, hence the scaling by c) include 73.2, 36.6, 18.3, $\cdots$ km s^{-1}, which match the common original periods very well. The next most common periods match the cube-root, $T = 6$ series. In the particle domain these are the sequences which associate with the proton and electron. The cube-root families are dominate, but redshifts within the ninth-root families do occur, especially $T = 1$, 5, and 7. The extreme dwarfs match the $T = 7$ family which incorporates the 10.67 km s^{-1} period found before values were predicted. Periods with $T = 2$, 4, or 8 are rare. A random accidental pattern should show no preferred T values.

The first reaction to the Lehto-Tifft cube-root rule is that it is unlike anything seen before. This is not the case, however, it is essentially Kepler's third law,

$$a^3 \alpha P^2 \quad a\alpha(P^2)^{1/3}.$$

The cubic term appears because space is 3-dimensional – potential goes as $1/r$, force as $1/r^2$, properties of a 3-d geometry. In a quantized temporal geometry 'a' is a quantized time interval. The rule implies the presence of a 3-d space, but our 1–d perceptional reduction prevents us from seeing 'lateral' effects where angular momentum enters (Kepler #3 contains #2 and #1). If some form of 'orbital' dynamics were to exist in 3-d temporal space we will see only the 'radial' interval directly and will infer Kepler's laws in inverse order. There are in fact patterns in the distribution of particle masses, and the forces governing them, that suggests that a 3-d temporal dynamical structure could exist involving both radial and azimuthal quantization at the Planck scale; perhaps we are 'linelanders' viewing 3-d temporal 'dynamics'. A 3-d temporal structure on macroscopic scales provides a completely new viewpoint for cosmology as well (Tifft 1996b).

The ninth-root rule for redshift periods admits many possible periods but only a few are common. They group into four sets and associate with four classes of galaxies. Table 1 summarizes the most important periods. The major $T = 0$ sequence, and some associated $T = 1$ periods, relate to the common spirals with intermediate to wide 21 cm profiles. Wide profile galaxies involve the sequence of short $T = 6$ periods and some $T = 0$ and $T = 3$ cube-root periods. Common dwarf galaxies, morphology $t = 9$ or 10, show longer $T = 6$ periods and some related $T = 5$ periods.

Table 1. Selected redshift periods $P = c2^{-(9D+T/9)}$.

$D\backslash T$	7	6	5	1	0
17	...	...	...	...	2.2872
16	2.6681	2.8817	...	...	4.5745
15	5.3363	5.7635	...	...	9.1490
14	10.6725	11.5270	...	16.9416	18.2979
13	...	...	...	33.8831	36.5958
12	...	46.1078	49.7992	...	73.1916
11	...	92.2157	99.5984	...	146.3833
10	...	184.4313	...	...	...

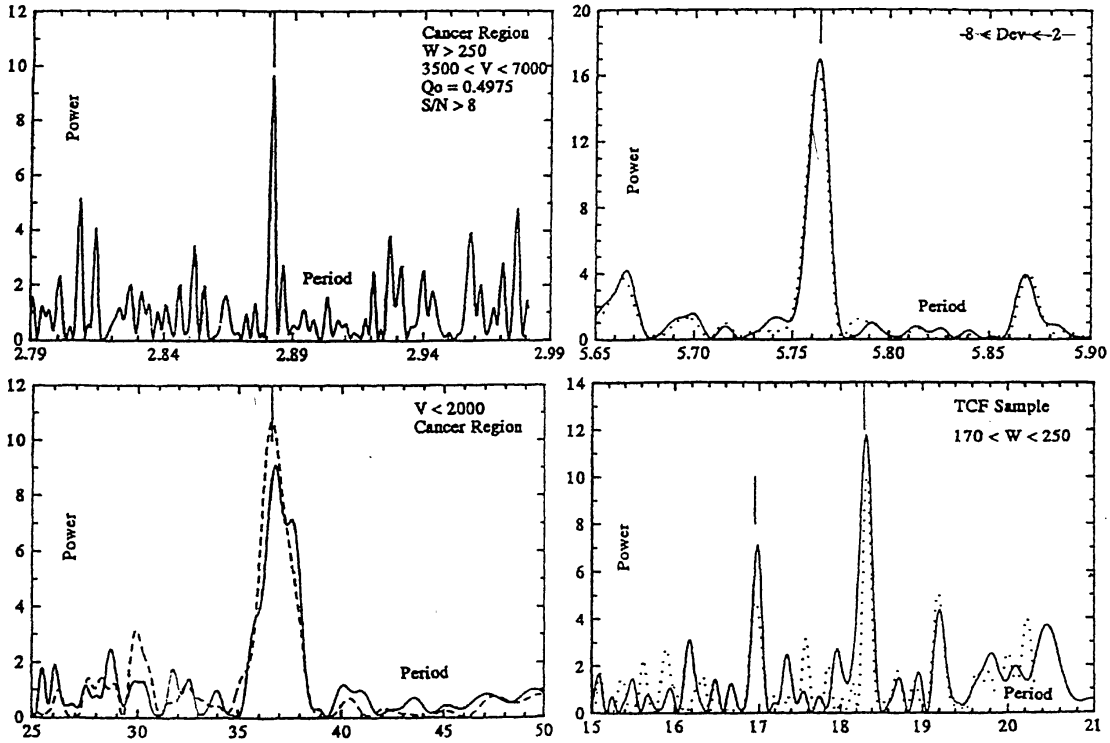

Figure 6. Power spectra of wide profile spiral galaxies (top) where short $T = 6$ periods are dominate, and ordinary intermediate width profile spirals (bottom) where $T = 0$ periods are dominate. The same T families occur in different regions. Cancer (left) and local (right) data are displayed here.

Extreme dwarfs with $W < 75\,\mathrm{km\,s^{-1}}$, populate the $T = 7$ sequence. Periods associated with $T = 2$, 4, or 8, are rare. Statistical testing assumes all periods are equally likely by accident. This is not the case, there is a regular pattern of uneven frequency and morphological association.

Figure 6 contains power spectra of the spiral families. Local supercluster galaxies in the Cancer region foreground (lower left) show the common strong $36.6\,\mathrm{km\,s^{-1}}$ $T = 0$ period. The more homogeneous the sample the higher the power and the better the fit to predictions (vertical line). At lower right we see the $18.3\,\mathrm{km\,s^{-1}}$ $T = 0$ period for local spirals in the Tifft-Cocke survey. Power rises as profile asymmetry is restricted; an associated $T = 1$ period is present. The upper frames show $T = 6$ spectra for the short periods in wide profile spirals. The samples shown here all appear in Fig. 5 where the CBR association is shown. A full description of these samples requires considerations of variability and cosmological corrections beyond the scope of this short review.

Phase-Deviation diagrams and a power spectrum for the two dwarf families of galaxies are shown in Fig. 7. These samples illustrate apparent redshift variability. Deviation is the redshift difference (Tifft-Cocke)–(Fisher-Tully) or Tifft-Cocke (1986–1984) at upper right. The upper frames show common dwarf galaxies where the longer $T = 6$ periods occur. A periodic deviation pattern, consistent with variability, is present and continues into the recent precision data. A double phase cycle brings out the periodic wave. Without using deviations this periodicity could not be seen; homogeneous accurate data at well defined epochs are essential for quantization

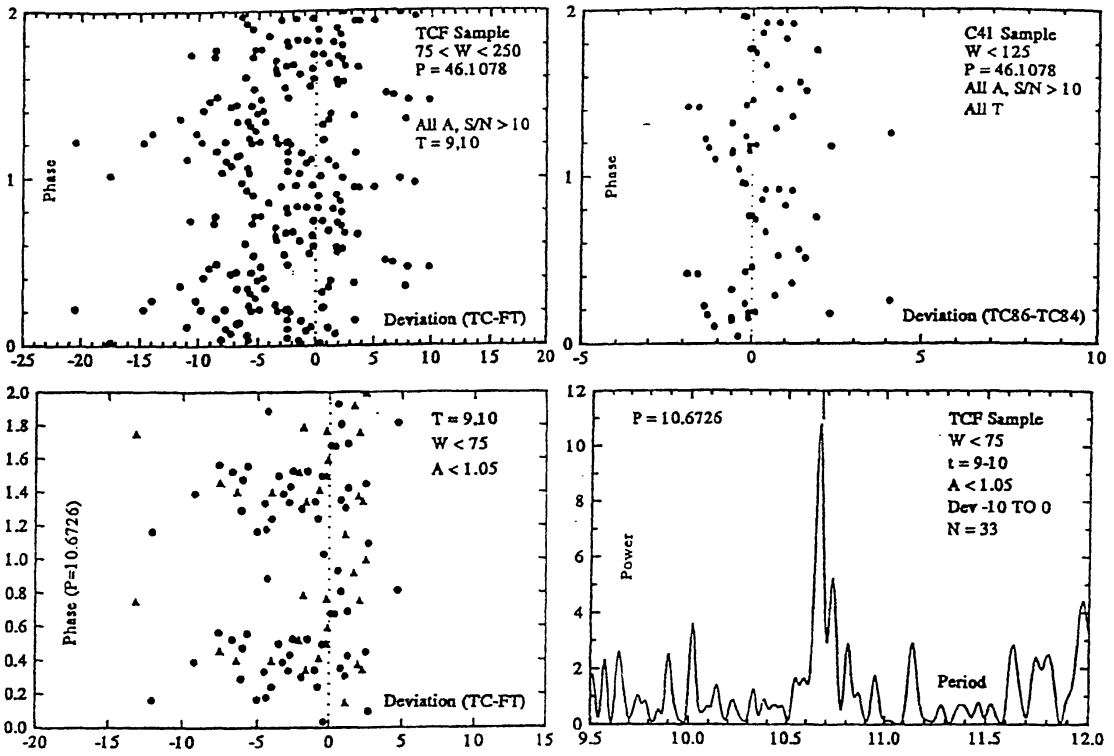

Figure 7. Phase-deviation diagrams (top) for dwarf galaxies with relatively wide profiles which have longer $T = 6$ periods and show deviations indicative of redshift variability. A phase-deviation diagram and a power spectrum (bottom) show the $T = 7$ periodicity characteristic of extreme dwarfs.

studies. The lower frames contain data for extreme dwarf galaxies where a strong deviation pattern appears at the $10{\cdot}67\,\mathrm{km\,s^{-1}}T = 7$ period. Asymmetry restrictions appear to distinguish possible stages within a changing pattern. The spectrum refers to the galaxies in the negative deviation wing; the association of this sample with the CBR vertex was shown in Fig. 5. Precisely tuned periods and deviations appear in specific classes of galaxies when the redshifts are transformed to the CBR rest frame. Galaxies in different regions and surveys have common properties.

4. The evidence for quantization in the CBR rest frame

In the introductory material we have already developed some of the key evidence in support of a quantized redshift. For details refer to Tifft (1996, 1996a, 1997)

- Periods are not arbitrary, they come from a precisely predicted set. They fall in classical period-doubling sets, not arbitrary patterns.
- Specific T values are preferred, first the basic powers of two, then other cube roots, odd ninth roots and finally even ninth roots in a distinctly non-arbitrary pattern. The preferred T values, 0 and 6, correspond to the particle mass series which contain the proton and electron
- Related sets of periods associate with specific classes of galaxies.
- Similar types of galaxies in different regions and samples show the same or simply related periodicities.

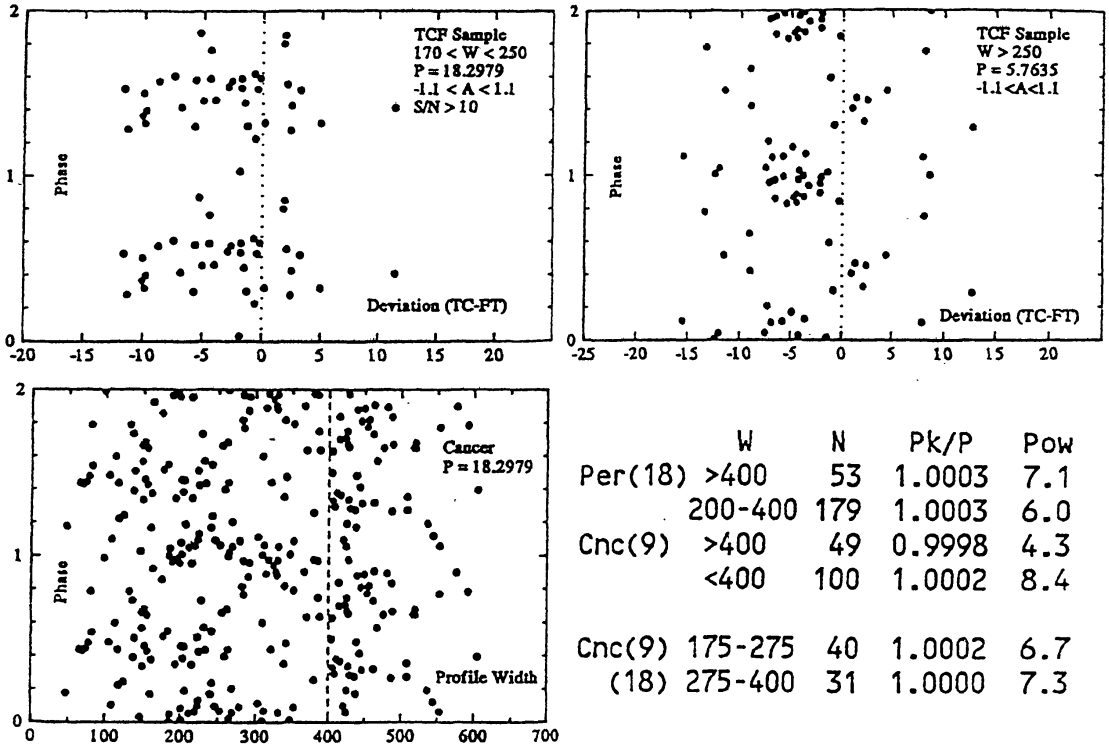

	W	N	Pk/P	Pow
Per(18)	>400	53	1.0003	7.1
	200-400	179	1.0003	6.0
Cnc(9)	>400	49	0.9998	4.3
	<400	100	1.0002	8.4
Cnc(9)	175-275	40	1.0002	6.7
(18)	275-400	31	1.0000	7.3

Figure 8. Phase-deviation diagrams for local galaxies, and a phase-width diagram for Cancer data, show the association of galaxies with simple fractions of absolute phase. The Cancer data and the inset table illustrate continuity in the fit to predicted periods between separate adjacent data sample.

- Many independent samples define the same CBR associated rest frame.

In Fig. 8 we look more closely at *phase relationships*. The figure contains phase-deviation diagrams for local galaxies with intermediate and wide profiles (top) which fit the $T = 0$ and $T = 6$ period families. At lower left a phase-width diagram is shown for a basic Cancer sample where the $T = 0$ family is strong.

- Phase concentrations are not arbitrary, the primary periodicities associate with simple phase fractions, .0, and .5 especially. The periodicities are *in phase* with the CBR rest frame, not arbitrary as an accidental association would predict.

A table inset at lower right in Fig. 8 summarizes some findings relating to *continuity* of periods (in parentheses after the region name) as a function of profile width. N is sample size, P_k/P the ratio of observed period to predicted period, and Pow the power at the observed period. Predicted periods are separated by a factor of 1.08 (the ninth-root of 2) if we ignore the fact that all T values are not equally likely. Random period matches should spread evenly over 1.00 ± 0.04 in P_k/P and show no T preference.

Two critical profile width intervals have been identified, near $W = 200$ and $400\,\mathrm{km\,s^{-1}}$ where distinct phase changes occur and/or a shift between harmonics in the same period family occurs.

- Periods and the CBR vertex fit (see Fig. 5 for Perseus) track smoothly across the phase/harmonic transition regions. Period matches track predicted periods within

1.0000 ± 0.0004 (within 1% of the random range allowed). The transition regions are the same for different regions and samples. This is extremely unlikely by accident.

Apparent variability in the redshift provides important evidence about the significance of quantization. Some simple examples have already been given. The same periods and phasing properties seen in single epoch data are found. We defer variability to the end of this report where it may be examined separately.

One special property which warrants mention relates to the cosmological correction applied to redshifts. The correction, (Tifft 1991), is a function of q_o, (not likely to have its usual meaning here), and is important for short periods in deep redshift samples. The non-linearity, to first order, stretches redshifts and shifts periods to longer values. The upper frame and inset table in Fig. 9 illustrates the effect of the correction.

- For independent samples locally, in Perseus and in Cancer, observed periods move into *precise* agreement with predicted values, (the P_k/P value passes through 1.00000), when q_o assumes the rather unique value 0.50. This is also the only value for which corrections can be derived in closed form.

We now turn to statistical tests of significance. More than 50 close matches at power above 4, usually well above 4 (which is already unlikely to occur at a specific predicted frequency at the $e^{-4} = 0.018$ level) are discussed in the most recent publication (Tifft 1996). Perhaps more interesting is the uniqueness of the association of power with the predicted periods. The lower part of Fig. 9 gives two examples. In

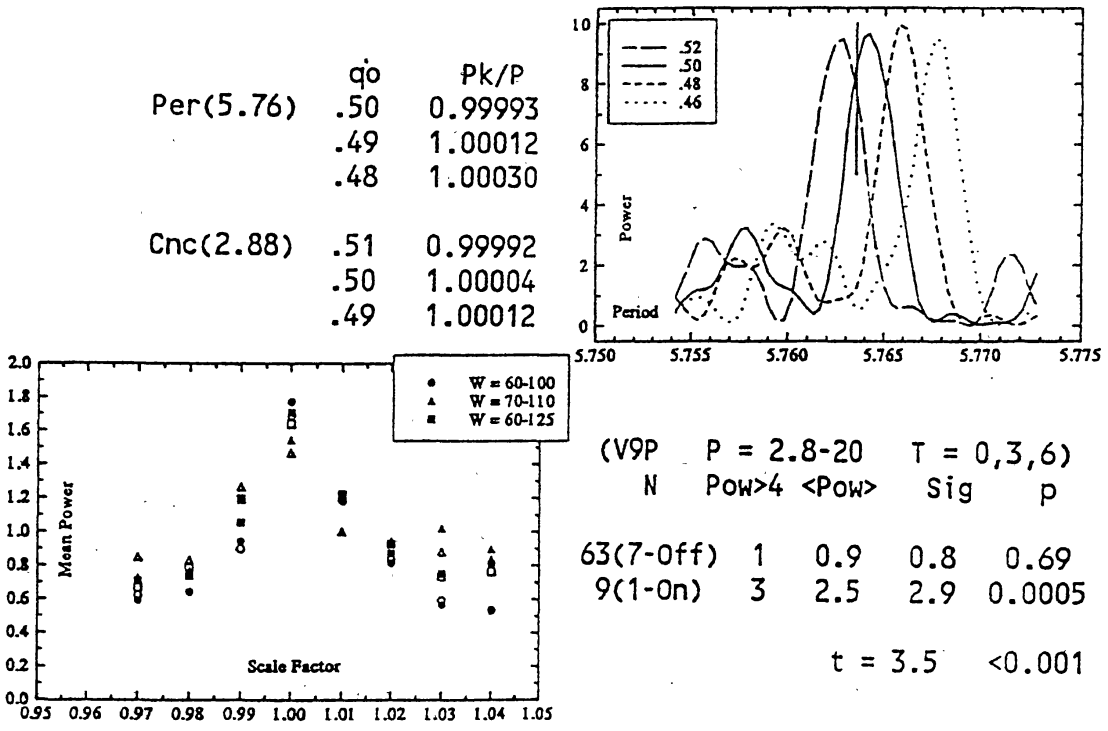

Figure 9. Power spectra and tabular examples (top) where cosmological corrections bring periods into precise match with predictions when $q_0 = 1/2$. The lower figure and table, illustrate that periods concentrate to the unique set of periods given by the ninth-root rule, (see text for descriptions).

the lower left frame the mean power over a range of possible periods is plotted, for three Virgo samples, against a scale factor which defines periods used. Factor 1.00 corresponds to the predicted set; power peaks uniquely at 1.00 and drops to a minimum midway between the predictions. Power dispersion does the same thing; a Student's t comparison shows clear significance.

In a table inset at lower right a local sample is examined for the most common cube root periods in the period range from 2.8 to 20 km s^{-1}. The same scaling shown in the Virgo diagram was used to generate 63 trials for the 9 possible periods at 7 off points, and 9 trials matching the one predicted set. The number of peaks found with power above 4, and the mean power and power dispersion in each set is given. A Student's t test comparing the means is shown at the bottom. Binomial test probabilities at the right evaluate the chance of hitting power 4 or above (probability $e^{-4} = 0.018$). One hit in 63 trials shows no evidence for periods away from predictions. Three hits in 9 trials is highly significant and again attests to the unique period set present.

In such samples it is often possible to show directly the presence of a non-exponential signal superposed on an exponential noise distribution. Still another test uses Student's t to compare mean deviations in absolute phase intervals as a demonstration of significance of staggered patterns in a variability analysis. An immense amount evidence exists which confirms quantization.

- High power is *uniquely* present at predicted periods even if we ignore the preference for certain T values. Significance does not depend upon power levels alone, it is established by the unique concentration of peaks at predicted locations and deviation patterns independent of spectral analysis.

We will close this review with a discussion of some evidence for, and properties of, redshift variability. The phase-deviation diagram in Fig. 10 illustrates the concept.

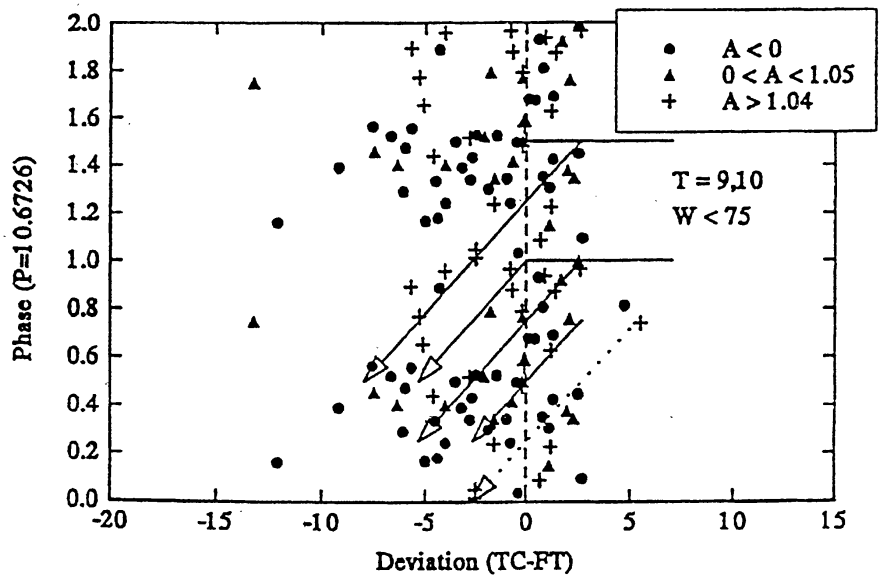

Figure 10. Phase-deviation diagram for extreme dwarf galaxies with hypothetical transition paths to indicate how cascades through higher harmonics could generate the staggered deviation patterns seen. Profile asymmetry appears to distinguish stages or timing within the cascade pattern.

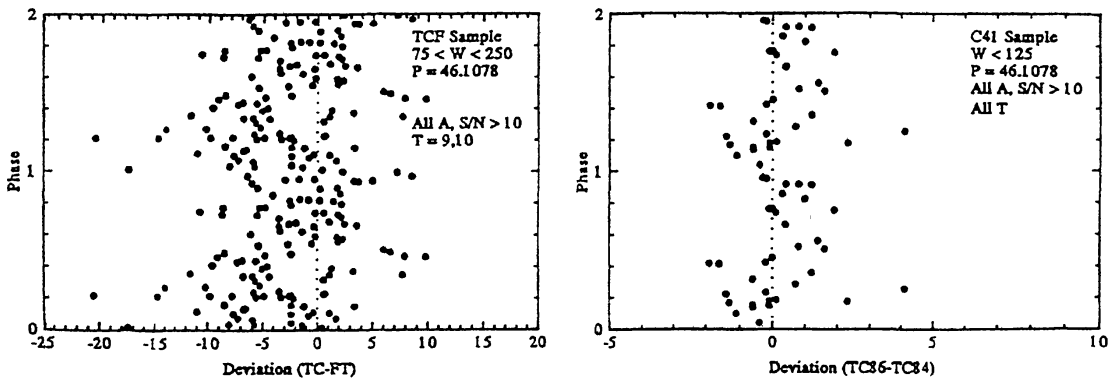

Figure 11. Phase-deviation diagrams for common dwarf galaxies where a staggered deviation pattern lets one see quantization even if no overall clumping appears in the phase distribution. In this case the variation appears to continue into the recent observations seen in the panel on the right.

Galaxies seem to cascade, in an interleaved pattern of subharmonics, between relatively stable low harmonics. If caught at the right stage we can get the prominent periodic deviations shown in Fig. 10, or the staggered patterns in Fig. 11 where intermediate levels mask any overall phase clumping. These two figures repeat from Fig. 7 except we have added positive asymmetry objects in Fig. 10 to show how they interleave with the symmetric and negative ones. Fig. 11 also shows that deviations appear to continue into newer data. They are not an artifact of the Fisher-Tully data alone.

The most remarkable example of apparent variability (Tifft 1997) is found, however, among local spiral galaxies in the $T = 0$ family. The top frame of Fig. 12 is a phase-deviation diagram of the complete set of 249 galaxies with Tifft-Cocke and Fisher-Tully redshifts and profiles between 100 and 300 km s^{-1} wide. It includes both dwarfs and spirals and maps into the 18.3 km s^{-1} period centered at phase 0.5 very well. The excellent CBR association of this complete sample was shown in Fig. 5 where power peaks close to 10. This group of objects falls in the 200 km s^{-1} profile width range where we noted a pattern of harmonic changes in very similar Cancer data. The region was in fact selected to specifically investigate the 200 km s^{-1} transition zone.

Individual data points in Fig. 12 are much more accurate than the scatter in phase would indicate. The scatter is due to underlying structure, as seen in Cancer, not uncertainties. The first step to see the structure involves removing the dwarfs which, although they generally show the 18.3 km s^{-1} period, have a relationship with the longer $T = 6$ periods not shared by the spirals. This leaves the lower frame of Fig. 12. Phase scatter remains, but deviation patterns emerge that resemble multiple cascade paths. The final step involves sorting the spirals by asymmetry; Positive asymmetry galaxies in the core of the transition pattern are shown in the center frame of Fig. 12. The resemblance to the asymmetry split in Fig. 10 is now apparent. Asymmetry seems to have the ability to distinguish the stages, or timing, within transitions. The local galaxies now reveal the same 9.15 km s^{-1} period mapped by the equivalent Cancer galaxies in the 200 km s^{-1} transition region. It is difficult to interpret these patterns any other way, but I am open to suggestions.

In Fig. 13 we replot a phase-deviation diagram for an enlarged sample of positive asymmetry spirals by extending widths to the 300 km s^{-1} bound of the original

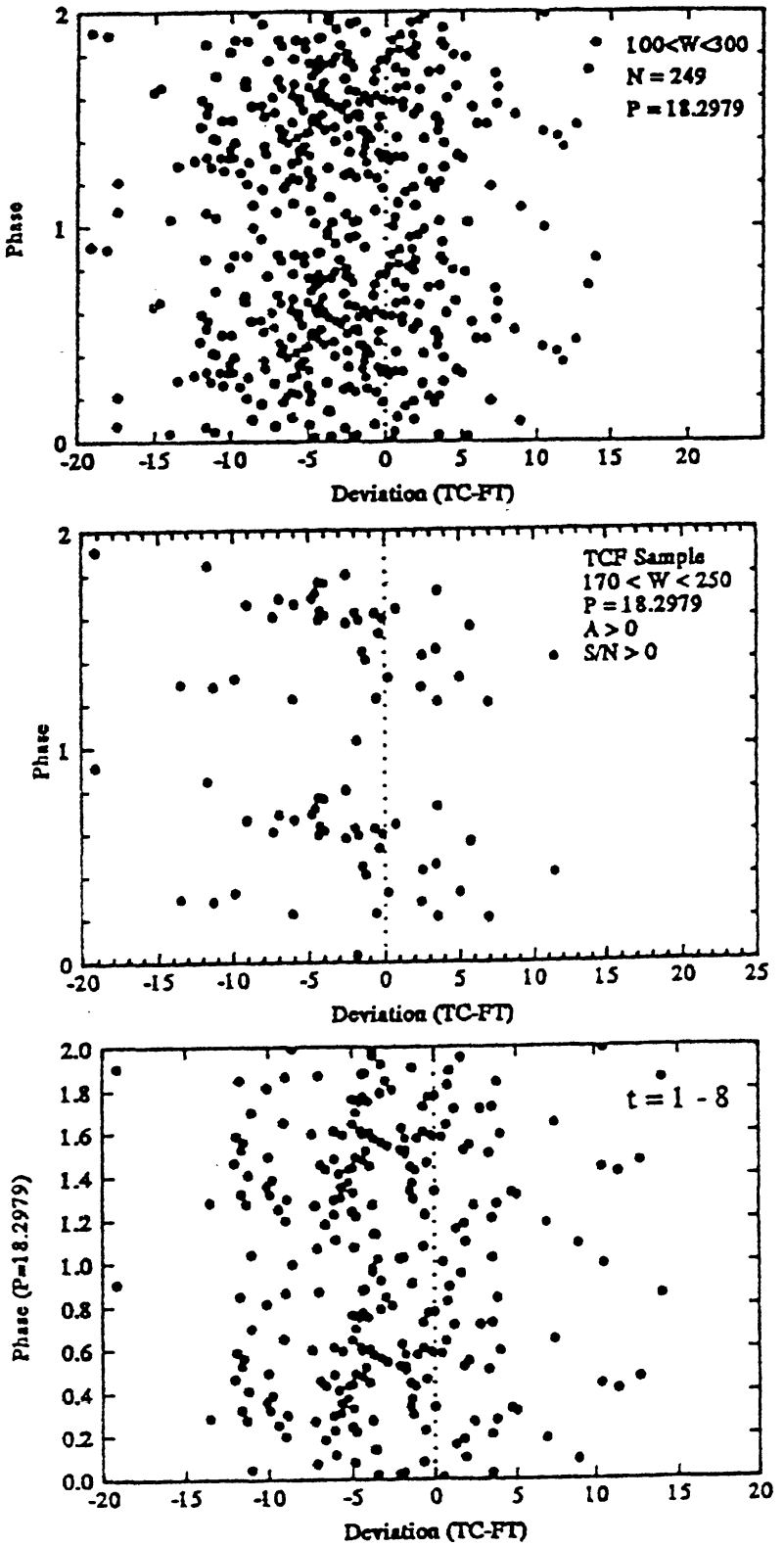

Figure 12. Phase deviation diagrams for local galaxies with intermediate width profiles. The total sample (top) contains a higher harmonic periodicity when sorted by asymmetry (center) and shows a cascade pattern in deviations when spiral galaxies are isolated by removing the dwarfs (bottom).

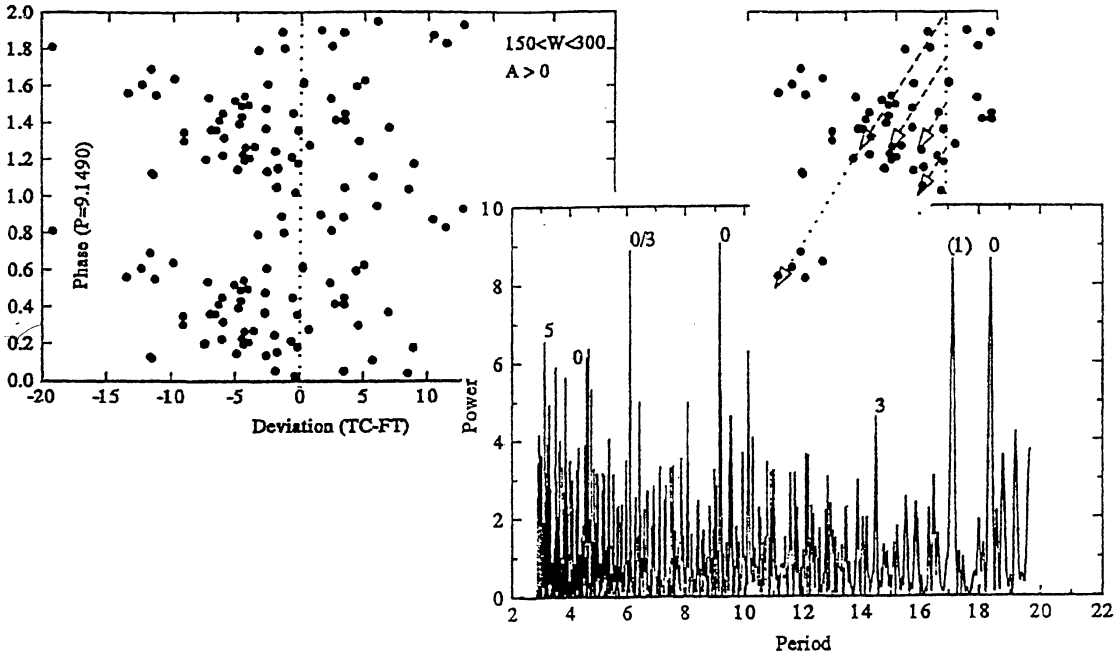

Figure 13. Phase deviation diagram (left) for positively asymmetric local galaxies with intermediate width profiles. The power spectrum (right) of the negative deviation wing shows a cascade structure (inset) of harmonics of the 18.3 km/s $T = 0$ period.

sample. We use the 9.15 km s^{-1} harmonic characterizing the group which we believe could represent a very homogeneous subsample of galaxies partaking in a fundamental $T = 0$ transition. The inset shows suggested cascades where we may be able to demonstrate paths down to the 2.8 km s^{-1} harmonic. The power spectrum of the core of the negative going deviation wing confirms our expectations; it shows the full set of harmonics, 18.3, 9.15, and 4.57 km s^{-1}, 1, 1/2, and 1/4 of 18.3 km s^{-1}. It also has the 1/3 harmonic which is automatically generated by a dispersed pattern of the 1/4 harmonics. This is the sample discussed in the uniqueness table within Fig. 9.

Table 2, looks at binomial probabilities for various ways of binning periods, limiting the period range, and setting the power cut. The number of peaks present (Pks), the number of matches (Hit), the probability of an accidental fit (p_H) and the number of roots considered, (all nine or only cube roots, and with or without the 1/3 match), determine the final binomial probability.

Table 3 shows how we can easily isolate the periodic signal from the random spectral noise. For various power cutoff levels, P, we have the random probability of accidental occurrence e^{-P}. The period range tested and the redshift range of the

Table 2. Binomial tests (* incl 1/3).

P	Cut	Pks	Hit	p_H	Rts	p	Meth
3–20	6	8	4	0.100	9	0.005	P.R.
4–20	6	7	3	0.100	9	0.02	
4–20	6	7	3	0.031	3	0.001	
4–20	6	7	3	0.043	3	0.002	S.M.
4–20	6	7	*4	0.045	3	0.0001	
4–20	4	15	*5	0.45	3	0.0004	

Table 3. Non-exponential signals.

Power >	4	5	6	8	Indep P
e^{-P}	0.018	0.0067	0.0025	0.0003	
Obs/Expec	20/14	12/15	8/2	4/0	770(P= 3–20)
Exc/Misft	6/12	7/5	6/2	4/0	Excess = 6
Obs/Expec	15/9	9/3	7/1	4/0	500(P = 4–20)
Exc/Misft	6/8	6/3	6/2	4/0	Excess = 6

sample give the number of independent periods the sample can contain. This number, given in the final column, times the accidental probability, gives the expected number of peaks above a given power due to noise. This is labeled 'Expec' for comparison with the actual count, 'Obs'. The difference is an excess, potentially real signal, 'Exc'. We confirm this by seeing that the actual number of real peaks in the spectrum which do *not* fit predictions, 'Misft', matches the noise expectation closely. There is an exponential noise component, as expected, and an excess signal, uniquely associated with the expected periods, which stands far above the noise.

This result, currently submitted for publication (Tifft 1997) marks the present bounds of redshift work. A detailed investigation of fundamental particles and forces will be included in an expanded form of this review being prepared for publication. The particles and forces are, if anything, proving even more interesting.

References

Beardsley, J. 1992, *Scientific American, Dec.*, p. 39.
Bicay, M., Giovanelli, R. 1986, *Astr. J.*, **91**, 705 & 732; 1987, *Astr. J.*, **93**, 1326.
Cocke, W. J., Tifft, W.G., 1996, *Astrophys. & Space Sci.*, **239**, 35.
Fisher, J. R., Tully, R. B., 1981, *ApJS*, **47**, 139.
Giovanelli, R., Haynes, M. P. 1895, *Astr. J.*, **90**, 2445; 1989, *Astr. J.*, **97**, 633.
Guthrie, B. N. G., Napier, W. N., 1991, *Mon. Not. R. Astr. Soc.*, **253**, 533.
Guthrie, B. N. G., Napier, W. N., 1996, *Astr. Astrophys.*, **310**, 353.
Hoffmann, G. L. *et al.*, 1987, *ApJS*, **63**, 247.
Lake R. G., Roeder R. C., 1972, *JRAS Canada*, **66**, 215.
Lehto, A., 1990, *Chinese J. Phys.*, **28**, 215.
Tifft, W. G., 1976, *Astrophys. J.*, **206**, 38.
Tifft, W. G., 1977a, *Astrophys. J.*, **211**, 31.
Tifft, W. G., 1977b, *Astrophys. J.*, **211**, 397.
Tifft, W. G., 1978, *Astrophys. J.*, **221**, 756.
Tifft, W. G., Cocke, W. J., 1984, *Astrophys. J.*, **287**, 492.
Tifft, W. G., 1988, *New Ideas in Astronomy*, (Cambridge), p 173.
Tifft, W. G., Cocke, W. J., 1988, *ApJS*, **67**, 1.
Tifft, W. G., Cocke, W. J., 1989, *Astrophys. J.*, **336**, 128 TC (pairs).
Tifft, W. G., 1990, *ApJS*, **73**, 603.
Tifft, W. G., Huchtmeier, W. K., 1990, *Astr. Astrophys. Suppl.*, **84**, 47.
Tifft, W. G., 1991, *Astrophys. J.*, **382** 396.
Tifft, W. G., 1991, *Astrophys. J.*, **368**, 383.
Tifft, W. G., 1995, *Astrophys. & Space Sci.*, **227**, 25.
Tifft, W. G., 1996, *Astrophys. J.*, **468**, 491.
Tifft, W. G., 1996a, *Astrophys. & Space Sci.*, **244**, 1/2 Time Conf proceedings, Kluwer 1997.
Tifft, W. G., 1996b, *Astrophys. & Space Sci.*, **244**, 1/2 Time Conf proceedings, Kluwer 1997.
Tifft, W. G., 1997, *Astrophys. J.*, **485**, 465.